PHYSICAL REVIEW B **91**, 201401(R) (2015)

Topological crystalline insulator and quantum anomalous Hall states in IV-VI-based monolayers and their quantum wells

Chengwang Niu,* Patrick M. Buhl, Gustav Bihlmayer, Daniel Wortmann, Stefan Blügel, and Yuriy Mokrousov
Peter Grünberg Institut and Institute for Advanced Simulation, Forschungszentrum Jülich and JARA, 52425 Jülich, Germany
(Received 27 February 2015; revised manuscript received 20 April 2015; published 5 May 2015)

Different from the two-dimensional (2D) topological insulator, the 2D topological crystalline insulator (TCI) phase disappears when the mirror symmetry is broken, e.g., upon placing on a substrate. Here, based on a new family of 2D TCIs—SnTe and PbTe monolayers—we theoretically predict the realization of the quantum anomalous Hall effect with a Chern number $\mathcal{C} = 2$ even when the mirror symmetry is broken. Remarkably, we also demonstrate that the considered materials retain their large-gap topological properties in quantum well structures obtained by sandwiching the monolayers between NaCl layers. Our results demonstrate that the TCIs can serve as a seed for observing robust topologically nontrivial phases.

DOI: 10.1103/PhysRevB.91.201401 PACS number(s): 73.22.−f, 73.21.Fg, 73.43.−f

The topological crystalline insulator (TCI) is a recently discovered class of quantum states with an insulating bulk energy gap and gapless edge or surface states [1]. Gapless edge or surface states of TCIs arise from the crystalline symmetry in contrast to that of the $\mathbb{Z}_2$ topological insulator (TI), where the reason for protection is time-reversal symmetry (TRS) [1–4]. The first proposal of a material class with TCIs was purely theoretically [2] and consequently TCIs were experimentally observed in three-dimensional (3D) IV-VI semiconductors SnTe [5], $Pb_{1-x}Sn_xSe$ [6], and $Pb_{1-x}Sn_xTe$ [7,8]. Later on, several transition metal oxides [9,10], Bi_2Te_3 [11], and heavy-fermion compounds [12,13] have been found to be 3D TCIs.

Rather recently, the TCI state has been theoretically predicted to occur in two dimensions (2D) in SnTe multilayers [14], PbSe monolayers [15], and graphene multilayers [16]. While the experimental progress in 3D TCIs was rapid [5–8,17], the 2D TCI phase disappears when placed on a substrate for further experimental investigation or device application due to the breaking of the mirror symmetry. Without the substrate, the freestanding film is usually hard to grow, which is also the main reason why 2D TIs were experimentally mainly established in HgTe/CdTe and InAs/GaSb quantum wells up to now [18,19]. Therefore, it is highly desirable to search for new materials and novel formation mechanisms which maintain the mirror symmetry of 2D TCIs.

TCIs bear great potential for the investigation of exotic phenomena [17,20–22], such as the large Chern number quantum anomalous Hall (QAH) effect [21,22]. The QAH state, which is characterized by a quantized charge conductivity without an external magnetic field, has topologically protected dissipationless chiral edge states and therefore is a good starting point to realize ultralow-power consumption electronics [23]. The TRS breaking in TIs provides a promising platform to investigate this striking topological phenomenon [24,25]. However, the Chern number of the TI-based QAH state is usually limited to $\mathcal{C} = 1$ [24–26] or $\mathcal{C} = 2$ [27,28]. In magnetically doped thin-film TCI SnTe, the QAH phase was predicted with the Chern number reaching as much as four [21,22]. The QAH phase with a large Chern number leads to multiple dissipationless edge channels that provide better ways to optimize electrical transport properties and could greatly reduce the contact resistance for circuit interconnects [21,28,29].

Here, based on density functional theory (DFT), we predict that SnTe and PbTe (001) monolayers are 2D TCIs. We expose our TCIs to an exchange field, which mimics the effect of magnetic adatoms or a substrate: While an in-plane exchange field destroys the TCI phase, it survives for an out-of-plane magnetization. Based on the considered materials, we demonstrate the feasibility of realizing a TCI-originated QAH phase with a high Chern number, which is very robust to mirror symmetry breaking and/or magnetization fluctuations. Remarkably, a range of 2D TCIs can be realized in $NaCl_{2N}(Sn/Pb)Te_1$ quantum wells with a single layer of SnTe or PbTe embedded in N layers of the widely used substrate NaCl [30] on both sides. These systems exhibit large topologically nontrivial energy gaps with a magnitude tunable by the NaCl thickness. Our findings pave the way to the utilization of TCIs as seed materials for arriving at robust topologically nontrivial phases.

The first-principles calculations have been performed using the full-potential linearized augmented-plane-wave method as implemented in the FLEUR code [31]. The self-consistent calculations with spin-orbit coupling (SOC) were carried out with a cutoff parameter $k_{\max}$ of 3.8 bohr^{-1}. The experimental lattice parameters were used for pristine Sn/PbTe systems, while those for quantum well structures were obtained using the Vienna *ab initio* simulation package (VASP) [32]. The generalized gradient approximation in parametrization of Perdew, Burke, and Ernzerhof (GGA-PBE) was used for the exchange correlation potential [33]. The maximally localized Wannier functions (MLWFs) were constructed using the WANNIER90 code [34,35].

Bulk SnTe and PbTe share the same face-centered-cubic NaCl-type structure with the band structure of SnTe at the L point inverted relative to PbTe [2,36], which results in the realization of a 3D TCI state in bulk SnTe and a 2D TCI state in SnTe multilayers [2,14]. On the other hand, PbTe both in bulk and in thin (001) films is in the normal insulator (NI) state [2]. Here, we focus on the (001)-oriented *monolayers* of SnTe and PbTe. In Fig. 1(a) the top view of such a 2D monolayer is shown, with Sn (Pb) and Te atoms forming two square sublattices positioned in the mirror plane $z = 0$.

*c.niu@fz-juelich.de

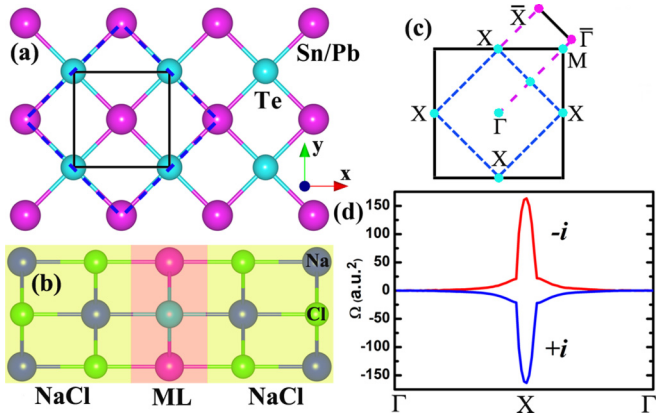

FIG. 1. (Color online) (a) Top view of the crystal structure of (001) Sn/PbTe monolayers with the unit cell and the $\sqrt{2} \times \sqrt{2}$ supercell indicated by black solid and blue dashed lines, respectively. (b) Schematic view of the $NaCl_{2N}(Sn/Pb)Te_1$ quantum well structure for $N = 2$. (c) Corresponding 2D Brillouin zones for the unit cell (solid square) and $\sqrt{2} \times \sqrt{2}$ supercell (dashed square), and projected 1D Brillouin zone with marked high symmetry points. (d) Berry curvature distribution associated with $\pm i$ mirror eigenstates of the occupied bands along the Γ-X-Γ path.

Accordingly, all Bloch states in the system can be labeled with the eigenvalues $\pm i$ of the reflection operator with respect to this symmetry plane.

To get preliminary insight into the topological properties of the systems, we present in Fig. 2 the orbitally resolved band structures of SnTe and PbTe monolayers with and without SOC. In the absence of SOC for SnTe, energy bands with the Sn-s and Te-p_y orbital character (positive parity with the inversion center at the Sn atom) overlap around the X point with the Sn-p_z states (negative parity). For PbTe at the X point without SOC a direct band gap appears with the valence band maximum (VBM) and the conduction band minimum (CBM)

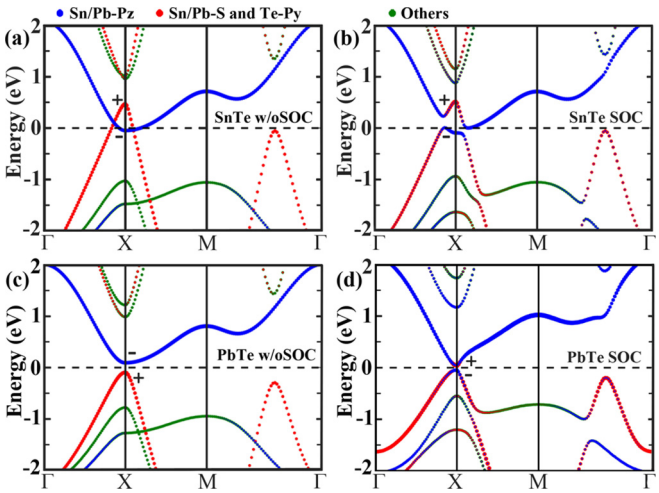

FIG. 2. (Color online) Orbitally resolved band structures for (001) monolayers of (a), (b) SnTe and (c), (d) PbTe, (a), (c) without and (b), (d) with SOC, weighted with the contribution of s, p_y, and p_z states. Parities of the conduction band minimum and valence band maximum at the X point are labeled by "+" and "−." The Fermi level is indicated with a dashed line.

dominated by the Pb-s and Te-p_y orbitals (positive parity), and the Pb-p_z orbital (negative parity), respectively. Turning on SOC leads to an insulating character in both systems (calculated band gaps are 0.05 eV for SnTe and 0.09 eV for PbTe), and to the band inversion in PbTe, so that with SOC the band structure is inverted in both systems.

Owing to an even number of X points in the Brillouin zone [see Fig. 1(c)], neither the SnTe monolayer nor the PbTe monolayer is a 2D TI. However, taking the mirror symmetry into account, similarly to bulk SnTe [2], for both SnTe and PbTe monolayers, band inversion results in the realization of a 2D TCI state. To show this explicitly, we calculate the so-called mirror Chern number $n_M = (n_{+i} - n_{-i})/2$, where n_{+i} and n_{-i} are Chern numbers of all occupied bands with opposite mirror eigenvalues $+i$ and $-i$, respectively [37]. The Chern number of a given subset of states is given by $\mathcal{C} = \frac{1}{2\pi} \int_{\mathrm{BZ}} \Omega(\mathbf{k}) d^2k$, where $\Omega(\mathbf{k})$ is the Berry curvature [38,39],

$$\Omega(\mathbf{k}) = \sum_{n<E_F} \sum_{m \neq n} 2\mathrm{Im} \frac{\langle \psi_{n\mathbf{k}} | \upsilon_x | \psi_{m\mathbf{k}} \rangle \langle \psi_{m\mathbf{k}} | \upsilon_y | \psi_{n\mathbf{k}} \rangle}{(\varepsilon_{m\mathbf{k}} - \varepsilon_{n\mathbf{k}})^2}, \quad (1)$$

with m,n as band indices which run over the considered subset of states, $\psi_{n\mathbf{k}}$ and $\varepsilon_{n\mathbf{k}}$ are corresponding Bloch states and their eigenenergies, and $\upsilon_{x/y}$ are the Cartesian components of the velocity operator. In Fig. 1(d), we plot the distribution of the Berry curvature of all occupied bands with a mirror eigenvalue $\pm i$. The main contribution to the Berry curvature comes from the region around X, with its values having an opposite sign for opposite eigenvalues. The Chern number for each polarization is, respectively, $n_{+i} = -2$ and $n_{-i} = 2$, yielding the total Chern number of all occupied states $\mathcal{C} = 0$ and the mirror Chern number $n_M = -2$. The calculated mirror Chern number $n_M = -2$ proves the TCI nature of (001)-oriented SnTe and PbTe monolayers.[1]

One of the prominent features of a TCI is the existence of gapless edge states that appear as a result of the crystal mirror symmetry only and do not require TRS [1,2]. To illustrate this, using a description in terms of MLWFs of 2D monolayers, we construct the tight-binding Hamiltonian of finite 80-atom wide ribbons oriented along the (110) axis [see the dashed lines in Fig. 1(a)]. In addition, by computing the matrix elements of the Pauli matrices $\sigma_\alpha (\alpha = x,y,z)$ in the basis of MLWFs, we consider the effect of an exchange field applied to our ribbon, which breaks the TRS and generally has out-of-plane ($\sigma_z \cdot B_\perp$ term in the Hamiltonian) and in-plane ($\sigma_x \cdot B_\parallel$ term) components. By introducing such an exchange field we aim at mimicking the effect of interactions with a magnetic environment, e.g., magnetic adatoms or a magnetic substrate [40].

The spin-resolved band dispersion of states localized at the "upper" ("lower") edge and the projected bulk band structure without any exchange field is presented in (the inset of) Fig. 3(a). Clearly, according to the mirror Chern number analysis, two pairs of edge states cross slightly away from

[1]The fact that in Ref. [14] only films thicker than four layers were found to be TCIs might be traced back to the fact that the film band structures were modeled from bulk DFT results in that work. Here, DFT calculations were performed explicitly for the films.

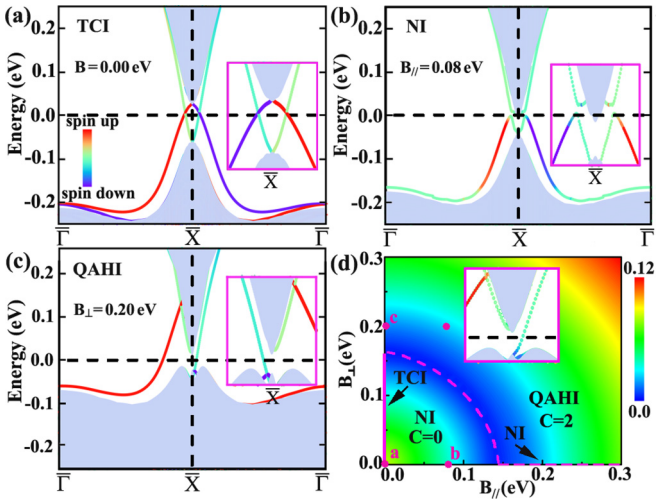

FIG. 3. (Color online) Evolution of the edge states of a (110)-oriented ribbon of a PbTe monolayer in an applied exchange field. (a) Upper edge without an exchange field ($B = 0.00$ eV, 2D TCI), (b) upper edge with an exchange field within the mirror plane ($B_{\parallel} = 0.08$ eV, NI), and (c) upper edge with an exchange field perpendicular to the mirror plane ($B_{\perp} = 0.20$ eV, QAHI). Edge states are colored with the expectation value of σ_z, as shown in (a). (d) Phase diagram of 2D PbTe with respect to $B_{\parallel}$ and $B_{\perp}$. The color scale represents the magnitude of the energy gap at the X point (in eV). The dashed line marks the phase boundary and the dots correspond to situations shown in (a)–(c). The inset in (d) shows the chiral edge states at the upper edge of the ribbon at a point in the phase diagram marked with a dot next to it.

the time-reversal invariant $\bar{X}$ point, and the spin polarization of the crossing states is of the same sign, which is in contrast to the case of 2D TIs. For an in-plane exchange field the mirror symmetry is broken and the edge states become gapped [Fig. 3(b)]. If the exchange field is, on the other hand, out of plane, the mirror symmetry survives and the system continues to exhibit gapless edge states, although the TRS is broken.

The TRS breaking causes an exchange splitting between conduction and valence bands of opposite spin, and thus, with increasing strength of the exchange field, they approach each other. As shown in Fig. 3(d), with increasing the magnitude of $B_{\perp}$, the band gap decreases with the system remaining a TCI, and it closes at around $B_{\perp} = 0.16$ eV, reopening again with further increasing $B_{\perp}$. According to our calculations, this signals a phase transition from a 2D TCI to a QAH phase, of which the latter is characterized by a nonzero Chern number of $\mathcal{C} = +2$. The nonzero Chern number is further verified by the presence of two gapless edge states on each side of the ribbon within the nontrivial band gap [see Fig. 3(c)].

Our most interesting finding is that the QAH state in our TCI system can be reached irrespective of whether or not the mirror symmetry is broken by $B_{\parallel}$, a topic that was addressed for 3D TCIs in Ref. [22] [see the computed phase diagram in Fig. 3(d) and its inset]. This means that TCIs can be used to arrive at different Chern insulators despite their apparent fragility to the mirror symmetry breaking, e.g., by a substrate. In fact, it is only the magnitude of the exchange field and not its direction to which the evolution of the topological band gap is sensitive, except for the situation with $B_{\perp} = 0$, when the system always resides in the NI state. Such a peculiar behavior also means that, when the QAH state is achieved in the system, it is not only robust with respect to the crystal symmetry, but also to the direction magnetization of adatoms or the substrate, which is subject to thermal fluctuations.

Finally, we choose the widely used material NaCl [30] to propose a practical way of stabilizing the 2D TCIs while keeping the mirror symmetry in $NaCl_{2N}(Sn/Pb)Te_1$ quantum wells. One of our main findings here is that the magnitude of the TCI band gap can be engineered by the thickness of the NaCl spacer, and it can reach as much as 0.13 and 0.47 eV in $NaCl_{2N}SnTe_1$ and $NaCl_{2N}PbTe_1$ wells, respectively. The sketch of the crystal structure of a $NaCl_{2N}(Sn/Pb)Te_1$ quantum well is shown in Fig. 1(b). A SnTe (PbTe) monolayer is placed in between N-layers-thick NaCl films, so that the mirror symmetry survives. When the SnTe (PbTe) monolayer is sandwiched between NaCl slabs, the interaction between SnTe (PbTe) and NaCl pushes the Sn/Pb-p_z orbital up in energy and Sn/Pb-s with Te-p_y orbitals down in energy at the X point. For the case of $N = 1$ the strongest interaction is observed, resulting in the disappearance of the band inversion and the TCI phase. With an increasing thickness of NaCl layers, the strength of the local potential decreases. Consequently, the band inversion and the TCI phase return at a critical NaCl thickness.

To show the thickness-dependent band inversion, we plot the orbitally resolved band structures in Figs. 4(a) and 4(b). We observe that, for small N, the Sn/Pb-s and Te-p_y orbitals contribute to the VBM with positive parity, while at larger NaCl thicknesses, they contribute to the CBM, keeping positive parity. Therefore, the band inversion occurs at $N = 2$ and

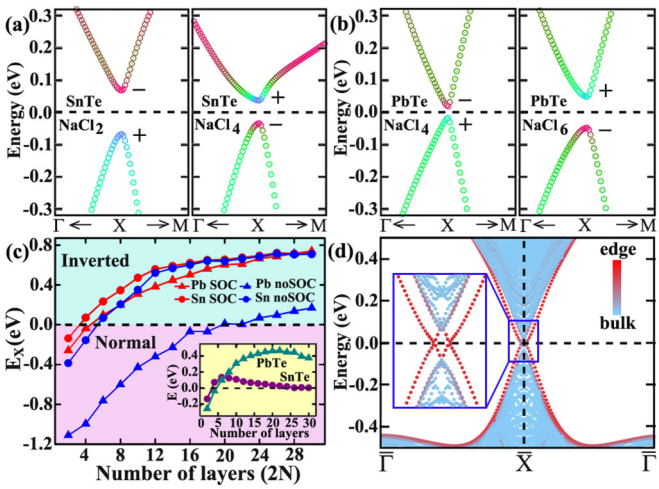

FIG. 4. (Color online) Orbitally resolved relativistic band structures of (a) $NaCl_{2N}SnTe_1$ and (b) $NaCl_{2N}PbTe_1$. Color from red to blue represents the increasing contributions of Sn/Pb-s and Te-p_y orbitals, which reveals the band inversion clearly. (c) Calculated energy gap of the $NaCl_{2N}(Sn/Pb)Te_1$ superlattice at the X point with and without SOC as a function of NaCl thickness. Negative and positive values correspond to the normal and inverted energy gaps, respectively. The inset shows the global energy gap as a function of NaCl thickness. (d) Localization-resolved band structure of a 1D nanoribbon of $NaCl_6PbTe_1$. The inset is the zoom-in at the $\bar{X}$ point.

$N = 3$ for the $NaCl_{2N}SnTe_1$ and $NaCl_{2N}PbTe_1$, respectively. Figure 4(c) shows the magnitude of the energy gaps at the X point without and with SOC versus the NaCl thickness. For $NaCl_{2N}SnTe_1$, the existence of the normal energy gap in both cases demonstrates a normal insulator phase for $N = 1$. For $N = 2$, a SOC-induced band inversion appears, indicating the realization of the 2D TCI phase. As the NaCl thickness increases further, the energy gap at the X point increases and the inverted energy gap is obtained even without SOC. Similar behavior is seen for $NaCl_{2N}PbTe_1$ with varying N, but the influence of SOC is more pronounced in this case. The 2D TCI state is further explicitly confirmed by the topological analysis and the emergence of the gapless edge states in 1D nanoribbons [see Fig. 4(d)]. The global energy gap is one of the defining properties of TCI. As shown in the inset of Fig. 4(c), the global gap survives for a large range of NaCl thicknesses, and its magnitude can be tuned by a proper choice of N, reaching as much as 0.13 and 0.47 eV for $NaCl_6SnTe_1$ and $NaCl_{22}PbTe_1$, respectively. Although inverted energy gaps are usually overestimated in DFT [41], our obtained values are probably large enough to ensure a robust TCI phase.

In summary, we have identified by first-principles calculations that the (001)-oriented SnTe and PbTe monolayers are topological crystalline insulators. We explore the phase diagram of these materials with respect to an applied exchange field due to magnetic adatoms or substrates. We show that as the mirror symmetry remains for the out-of-plane magnetization, the gapless edge states survive, but the TCI state is destroyed for an in-plane exchange field. For finite $B_\perp$, upon reaching a certain strength of the exchange field, we show the emergence of a robust Chern insulator phase which survives irrespective of the mirror symmetry breaking. We further show that the large-gap TCI Pb/SnTe based family can be successfully stabilized in $NaCl_{2N}(Sn/Pb)Te_1$ quantum wells. Especially for $NaCl_{22}PbTe_1$, a large energy gap of 0.47 eV appears.

Note added. Recently, we became aware of an independent work on the prediction of monolayer IV-VI semiconductors as TCI [42].

We are grateful to Hongbin Zhang for insightful discussions. This work was supported by the Priority Program 1666 of the German Research Foundation (DFG), the Virtual Institute for Topological Insulators (VITI), and the Project No. VH-NG-513 of the Helmholtz Association (HGF). We acknowledge computing time on the supercomputers JUQUEEN and JUROPA at Jülich Supercomputing Centre and JARA-HPC of RWTH Aachen University.

[1] L. Fu, Phys. Rev. Lett. **106**, 106802 (2011).
[2] T. H. Hsieh, H. Lin, J. Liu, W. Duan, A. Bansil, and L. Fu, Nat. Commun. **3**, 982 (2012).
[3] M. Z. Hasan and C. L. Kane, Rev. Mod. Phys **82**, 3045 (2010).
[4] X. L. Qi and S. C. Zhang, Rev. Mod. Phys. **83**, 1057 (2011).
[5] Y. Tanaka, Z. Ren, T. Sato, K. Nakayama, S. Souma, T. Takahashi, K. Segawa, and Y. Ando, Nat. Phys. **8**, 800 (2012).
[6] P. Dziawa, B. J. Kowalski, K. Dybko, R. Buczko, A. Szczerbakow, M. Szot, E. Łusakowska, T. Balasubramanian, B. M. Wojek, M. H. Berntsen, O. Tjernberg, and T. Story, Nat. Mater. **11**, 1023 (2012).
[7] S.-Y. Xu, C. Liu, N. Alidoust, M. Neupane, D. Qian, I. Belopolski, J. D. Denlinger, Y. J. Wang, H. Lin, L. A. Wray, G. Landolt, B. Slomski, J. H. Dil, A. Marcinkova, E. Morosan, Q. Gibson, R. Sankar, F. C. Chou, R. J. Cava, A. Bansil, and M. Z. Hasan, Nat. Commun. **3**, 1192 (2012).
[8] C. Yan, J. Liu, Y. Zang, J. Wang, Z. Wang, P. Wang, Z.-D. Zhang, L. Wang, X. Ma, S. Ji, K. He, L. Fu, W. Duan, Q.-K. Xue, and X. Chen, Phys. Rev. Lett. **112**, 186801 (2014).
[9] M. Kargarian and G. A. Fiete, Phys. Rev. Lett. **110**, 156403 (2013).
[10] T. H. Hsieh, J. Liu, and L. Fu, Phys. Rev. B **90**, 081112(R) (2014).
[11] T. Rauch, M. Flieger, J. Henk, I. Mertig, and A. Ernst, Phys. Rev. Lett. **112**, 016802 (2014).
[12] H. Weng, J. Zhao, Z. Wang, Z. Fang, and X. Dai, Phys. Rev. Lett. **112**, 016403 (2014).
[13] M. Ye, J. W. Allen, and K. Sun, arXiv:1307.7191.
[14] J. Liu, T. H. Hsieh, P. Wei, W. Duan, J. Moodera, and L. Fu, Nat. Mater. **13**, 178 (2014).
[15] E. O. Wrasse and T. M. Schmidt, Nano Lett. **14**, 5717 (2014).
[16] M. Kindermann, arXiv:1309.1667.
[17] Y. Okada, M. Serbyn, H. Lin, D. Walkup, W. Zhou, C. Dhital, M. Neupane, S. Xu, Y. J. Wang, R. Sankar, F. Chou, A. Bansil, M. Z. Hasan, S. D. Wilson, L. Fu, and V. Madhavan, Science **341**, 1496 (2013).
[18] M. König, S. Wiedmann, C. Brüne, A. Roth, H. Buhmann, L. Molenkamp, X.-L. Qi, and S.-C. Zhang, Science **318**, 766 (2007).
[19] I. Knez, R. R. Du, and G. Sullivan, Phys. Rev. Lett. **107**, 136603 (2011).
[20] E. Tang and L. Fu, Nat. Phys. **10**, 964 (2014).
[21] C. Fang, M. J. Gilbert, and B. A. Bernevig, Phys. Rev. Lett. **112**, 046801 (2014).
[22] F. Zhang, X. Li, J. Feng, C. Kane, and E. Mele, arXiv:1309.7682.
[23] F. D. M. Haldane, Phys. Rev. Lett. **61**, 2015 (1988).
[24] R. Yu, W. Zhang, H. Zhang, S. Zhang, X. Dai, and Z. Fang, Science **329**, 61 (2010).
[25] C. Z. Chang, J. Zhang, X. Feng, J. Shen, Z. Zhang, M. Guo, K. Li, Y. Ou, P. Wei, and L. L. Wang, Science **340**, 167 (2013).
[26] C. Niu, G. Bihlmayer, H. Zhang, D. Wortmann, S. Blügel, and Y. Mokrousov, Phys. Rev. B **91**, 041303(R) (2015).
[27] H. Zhang, F. Freimuth, G. Bihlmayer, S. Blügel, and Y. Mokrousov, Phys. Rev. B **86**, 035104 (2012).
[28] J. Wang, B. Lian, H. Zhang, Y. Xu, and S.-C. Zhang, Phys. Rev. Lett. **111**, 136801 (2013).
[29] S. A. Skirlo, L. Lu, and M. Soljačić, Phys. Rev. Lett. **113**, 113904 (2014).
[30] J. N. Zemel, J. D. Jensen, and R. B. Schoolar, Phys. Rev. **140**, A330 (1965).
[31] www.flapw.de
[32] G. Kresse and J. Furthmüller, Phys. Rev. B **54**, 11169 (1996).
[33] J. P. Perdew, K. Burke, and M. Ernzerhof, Phys. Rev. Lett. **77**, 3865 (1996).
[34] A. A. Mostofi, J. R. Yates, Y.-S. Lee, I. Souza, D. Vanderbilt, and N. Marzari, Comput. Phys. Commun. **178**, 685 (2008).

[35] F. Freimuth, Y. Mokrousov, D. Wortmann, S. Heinze, and S. Blügel, Phys. Rev. B **78**, 035120 (2008).

[36] C. Niu, Y. Dai, Y. Ma, L. Yu, and B. Huang, Mater. Express **3**, 159 (2013).

[37] J. C. Y. Teo, L. Fu, and C. L. Kane, Phys. Rev. B **78**, 045426 (2008).

[38] D. J. Thouless, M. Kohmoto, M. P. Nightingale, and M. den Nijs, Phys. Rev. Lett. **49**, 405 (1982).

[39] Y. Yao, L. Kleinman, A. H. MacDonald, J. Sinova, T. Jungwirth, D. S. Wang, E. Wang, and Q. Niu, Phys. Rev. Lett. **92**, 037204 (2004).

[40] M. Inoue, K. Isgii, and H. Yagi, J. Phys. Soc. Jpn. **43**, 903 (1977).

[41] I. Aguilera, C. Friedrich, G. Bihlmayer, and S. Blügel, Phys. Rev. B **88**, 045206 (2013).

[42] J. Liu, X. Qian, and L. Fu, Nano Lett. **15**, 2657 (2015).